Widely tunable frequency conversion in monolithic semiconductor waveguides at 2.4 μm

Payam Abolghasem, Dongpeng Kang, Dylan F. Logan, Mandy Lungwitz, and Amr S. Helmy*

The Edward S. Rogers Sr. Department of Electrical and Computer Engineering and the Institute for Optical Sciences, University of Toronto, Toronto, Ontario M5S 3G4, Canada

**Corresponding author: a.helmy@utoronto.ca*

Received March 21, 2014; revised May 11, 2014; accepted May 11, 2014; posted May 15, 2014 (Doc. ID 207454); published June 11, 2014

We report on the generation of continuous-wave widely tunable light between 2360 and 2530 nm using difference-frequency generation with a pump tuned between 938 and 952 nm and a signal tuned between 1490 and 1590 nm in a type-II phase-matched monolithic semiconductor waveguide. The device internal conversion efficiency is estimated to be 0.29% W^{-1} cm^{-2}. This design which uses a single-sided Bragg reflection waveguide has the potential for on-chip spectroscopy, as well as environmental monitoring applications, where a tunable source of coherent radiation tuned between 2 and 3 μm wavelength is desired.

OCIS codes: (190.4410) Nonlinear optics, parametric processes; (190.4390) Nonlinear optics, integrated optics; (130.7405) Wavelength conversion devices.

http://dx.doi.org/10.1364/OL.39.003591

There is an increasing demand for continuous-wave (CW) light sources emitting within the 2–3 μm region of the infrared (IR) spectrum with high spectral brightness. These source play a pivotal role in enabling high resolution, high sensitivity chemical sensing, and environmental monitoring applications. Certain molecules containing carbon-hydrogen bonds, such as CH_4 (2.35 μm) and ethylene C_2H_4 (2.9 μm) have IR footprints within the 2–3 μm spectral window. Pollutant agents and combustion products, including NH_3 (2.1 μm), HF (2.5 μm), and CO (2.3 μm) also exhibit strong absorption lines in this spectral range [1]. In addition, H_2O possesses significant absorption features around 2.5 μm, which can be used for *in situ* combustion measurements of moisture and temperature [2].

Several technologies have been perused to develop compact, cost efficient and robust sources to cover the 2–3 μm wavelength range. Diode lasers based on GaSb have been successfully demonstrated for lasing above 2 μm [3,4]. While quantum-cascade lasers (QCLs) are the dominant technology for mid-IR light generation above 3 μm, they face significant challenges in accessing the 2–3 μm spectral window when operating at room temperature [5,6]. In recent progress, demonstrated sources for this wavelength range using QCLs have been enabled using an up-conversion process, where the emission of the laser is frequency doubled to generate a 2.7 μm wavelength [7]. Fiber lasers based on ZBLAN or silicate fibers doped with elements including Tm^{3+}, Ho^{3+}, Pr^{3+}, and Er^{3+} have been utilized for generation of tunable IR radiation between 2 and 3 μm [8]. Another technique that can be used for these sources utilizes difference-frequency generation (DFG) in ferroelectric crystals such as $LiNbO_3$ [9] and in III–V compounds such as GaAs [10,11]. Using DFG in semiconductor devices is particularly attractive as the same semiconductor platform can also be used to build active devices, hence enabling the monolithic integration of a pump source with the frequency mixing element for an ultimately compact and monolithic source.

In this Letter, we demonstrated DFG around 2450 nm light (idler) by frequency mixing two near-IR wavelengths, namely 945 nm (pump) and 1550 nm (signal) in AlGaAs/GaAs Bragg reflection waveguides (BRWs) [12]. DFG of a signal and idler around 1550 nm has been previously demonstrated in BRWs using a symmetric geometry where the top and bottom cladding layers of the waveguide were composed of identical Bragg mirrors [13]. Here, we demonstrate nondegenerate DFG in a new class of BRWs, single-sided BRWs (SS-BRWs), where the Bragg mode (photonic bandgap mode) is confined by a Bragg mirror in the bottom cladding while it is evanescent in the top cladding [14]. The benefit of using SS-BRW is many folded. First, the existence of the evanescent field in the upper cladding provides a route for off-plane preferential coupling using grating couplers. Second, as the structure has only one Bragg mirror separating the waveguide core from the substrate, the overall epitaxial thickness is reduced enabling a better waveguide design with more feasible epitaxial growth. Third, as SS-BRWs have fewer layers of AlGaAs with different Al compositions, the propagation losses associated with scattering at various interfaces is reduced. Finally, SS-BRWs can be designed as lasers, where the thinner epitaxial structure along with the reduced number of interfaces between adjacent layers improves the electrical and thermal properties of this class of lasers.

The process of DFG involves the frequency-mixing of pump photons at wavelength λ_p, signal at λ_s and idler at λ_i. Conservation of energy requires that $\lambda_i^{-1} = \lambda_p^{-1} - \lambda_s^{-1}$. For appreciable power conversion into the signal and idler, a phase-matching (PM) condition should be satisfied. The PM condition is: $\Delta\beta = \beta_p - \beta_s - \beta_i = 0$, where $\beta_{p,s,i}$ are the propagation constants of the pump, signal, and idler modes. In a SS-BRW which is utilized in this work, the pump mode is a Bragg mode, and the signal and idler waves are modes that are guided by total internal reflection (TIR). The device was designed for type-II DFG with a TE pump at 930 nm, a TM signal at 1550 nm, and a TE idler at 2325 nm. A type-II process was the preferred PM scheme because it benefits from enhanced effective nonlinearity when compared to type-0 and type-I processes [15].

The wafer was grown on a GaAs wafer by metal organic chemical vapor deposition. The lower cladding

Bragg reflector was composed of five periods of $Al_{0.24}Ga_{0.76}As/Al_{0.61}Ga_{0.39}As$ with thicknesses 189/773 nm. The multi-layered core was composed of $Al_{0.53}Ga_{0.47}As/GaAs$ with thicknesses 562/293 nm. The upper cladding was 800 nm thick $Al_{0.85}Ga_{0.15}As$. The two-layered core was separated from the bottom Bragg mirror by a matching layer of $Al_{0.34}Ga_{0.66}As$ with a thickness of 661 nm. Ridge waveguides with a width of 4 μm and a depth of 810 nm were fabricated using plasma etching. The characterized devices had a length of 3.8 mm. The simulated field profiles at λ_p, λ_s and λ_i along with the an index profile of the structure are shown in Fig. 1.

The waveguide characterization was performed using a free-space optical setup involving end-fire coupling of the waveguide. A tunable CW Ti:Sapph laser centered around 945 nm was used as the pump, and an external cavity CW laser tunable between 1490 and 1590 nm was used as the signal. The two laser beams were set to be TE and TM polarized, respectively, by two polarization beamsplitters before they were combined into one optical path using a broadband beamsplitter. The combined pump and signal beam was subsequently coupled into the waveguide using a 40× objective lens (Newport, F-L40B). A Mid-IR ZnSe objective lens (Innovation Photonics, LFO-5-6) was used to collect the output light from the waveguide to a thermo-electrically cooled PbS detector (Electro-Optical Systems Inc., PBS-020-TE2-H) operating at –30°C, with the transmitted pump and signal removed by three long pass filters. To enhance the signal-to-noise ratio of the idler detection, a phase-sensitive detection setup with a lock-in amplifier was used, where the signal beam was chopped at a reference frequency of 200 Hz.

The coupling efficiencies into the pump and signal modes in the waveguide were estimated to be 4.4% and 32%, respectively, after taking into account the mode spatial overlaps and facet reflections. The low coupling efficiency for the pump is because of the small spatial overlap between the input Gaussian beam and the pump Bragg mode. Linear characterization of the device was carried out using the Fabry–Perot method at the signal wavelength around 1550 nm. The signal propagation loss was measured to be 1.9 cm^{-1}. The propagation loss in symmetric BRWs has been previously reported in [15] where the losses around 1550 nm wavelength were measured to be 2.2 and 2.4 cm^{-1} for TE and TM polarizations, respectively. The BRW device under test here shows a moderate reduction in the propagation loss which was expected as a result of using a single-stack BRW design with less dielectric interfaces and improved growth quality.

The dependence of the idler power on the pump wavelength for signal wavelengths of 1490, 1550, and 1590 nm are shown in Figs. 2(a), 2(b), and 2(c), respectively, with fixed pump and signal powers. The pump power before the input objective lens was fixed at 34.5 mW for all three cases, while the signal powers were fixed at 0.45, 23, and 0.22 mW, respectively. For the signal wavelength of 1550 nm, a C-band erbium-doped fiber amplifier was added to amplify the available signal power to obtain a

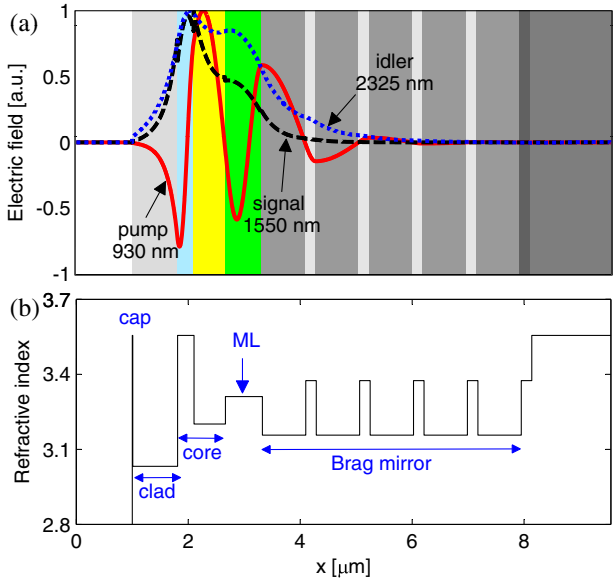

Fig. 1. (a) Electric field profiles of the TE pump (solid-line), TM signal (dashed-line), and TE idler (dotted-line) in the DFG device. (b) Refractive index profile of the device at pump wavelength.

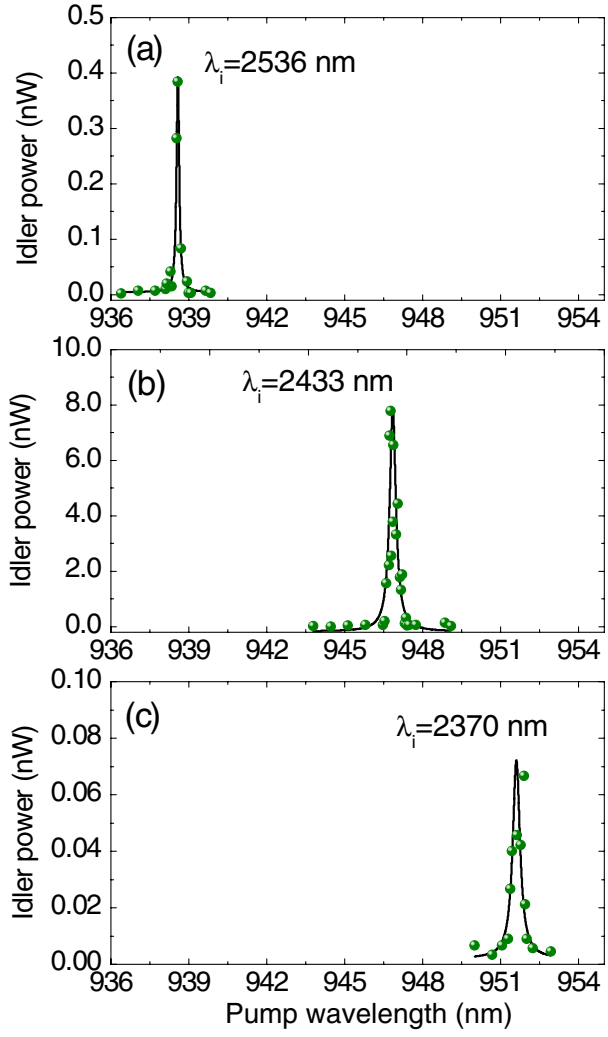

Fig. 2. Dependence of the idler power on the pump wavelength for fixed signal wavelengths at (a) 1490 nm, (b) 1550 nm, and (c) 1590 nm, respectively.

higher signal to noise ratio. This resulted in a maximum idler power of 7.8 nW detected at the detector. From Fig. 2, DFG resonances around 938.5, 947.0, and 951.6 nm are discernible, indicating a phase-matched process. The pump full-width at half-maximum wavelength acceptance bandwidth of the DFG process was measured to be ~0.5 nm. The measured PM wavelength is significantly different from that of the design, this is due to the shift in effective mode indices of the pump, signal, and idler as a result of ridge confinement as well as the inaccuracy in the refractive index model used in the design, particularly at the pump wavelength with proximity to material bandgap.

Figure 3 shows the variations of detected idler powers on those of the input pump and signal. From the figure, linear relations hold for both pump and signal powers. According to Fig. 3(a), a larger fluctuation of the idler power as the pump power increases can be observed, when compared with that of the signal in Fig. 3(b). This can be explained by the change of refractive index caused by absorption and heating from the pump, as the pump wavelength is close to the material bandgap. As the refractive index changes, the locations of Fabry–Perot resonances from the waveguide facets will shift, causing a fluctuation of the output idler power.

In another measurement, the wavelength tunability of the idler was examined by varying the signal wavelength between 1490 and 1590 nm and sweeping the pump wavelength to obtain PM point. The resulting tuning curve is shown in Fig. 4, where the section of the figure related to idler wavelength was extracted theoretically using energy conservation, i.e., $1/\lambda_i = 1/\lambda_p - 1/\lambda_s$. According to Fig. 4, variations of the signal and pump wavelengths by 100 and 13.4 nm, respectively, resulted in an idler span of 170 nm.

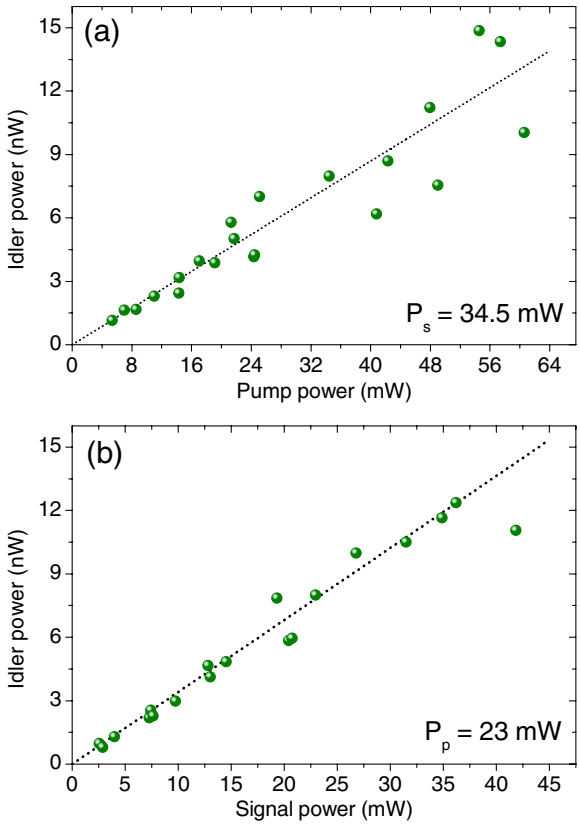

Fig. 3. Dependence of the idler power on (a) the pump and (b) the signal powers.

A figure of merit that indicates the performance of a DFG device is the internal conversion efficiency, defined as $\eta = P_i/(P_p P_s)$, where P_p, P_s and P_i are the pump, signal, and idler powers estimated inside the device. Taking into account the input pump and signal coupling efficiencies, and the output idler transmission coefficients from the waveguide facet (70%), objective lens (91%), and the long-pass filters (95% × 3), the internal efficiency was estimated to be $4.1 \times 10^{-2}\%\ \mathrm{W}^{-1}$. The corresponding normalized efficiency, is defined as $\eta_{\mathrm{norm}} = P_i/(P_p P_s L^2)$, was $0.29\%\ \mathrm{W}^{-1}\,\mathrm{cm}^{-2}$, where $L = 3.8$ mm is the waveguide length. The comparison between the DFG efficiency of the device reported here with other AlGaAs devices phase-matched using other techniques is noteworthy. For example, in an early work in form birefringence PM using GaAs/AlO_x waveguides, a DFG with an efficiency of $3\%\ \mathrm{W}^{-1}\,\mathrm{cm}^{-2}$ around 4 μm wavelength was measured using CW pump and signal at 1 and 1.32 μm [16] which was an order of magnitude more efficient than that of the devices here. In addition, the DFG has been demonstrated in orientation-patterned GaAs (OP-GaAs) for generation of mid-IR light. In [17], an OP-GaAs sample with a length of 19 mm has been demonstrated to generate and idler around 8 μm with a power of 38 nW by mixing a pump and signal at 1.3 μm (2.3 mW) and 1.55 μm (555 mW), respectively, with an extracted DFG efficiency of $8.2 \times 10^{-2}\%\ \mathrm{W}^{-1}\,\mathrm{cm}^{-2}$. Recently, a 1.2 mm long suspended GaAs wavelength has been demonstrated for generation of an idler between 2800 and 3150 nm through the DFG of a tunable pump between 1018 and 1032 nm and a signal between 1490 and 1620 nm [18]. We found the extracted conversion efficiency of this device to be $\approx 2.8 \times 10^{3}\%\ \mathrm{W}^{-1}\,\mathrm{cm}^{-2}$.

In summary, we demonstrated the generation of tunable light between 2360 and 2530 nm using a type-II DFG process in a monolithic semiconductor waveguide with the pump between 938 and 952 nm and signal around 1490–1590 nm. The wide wavelength tunability of

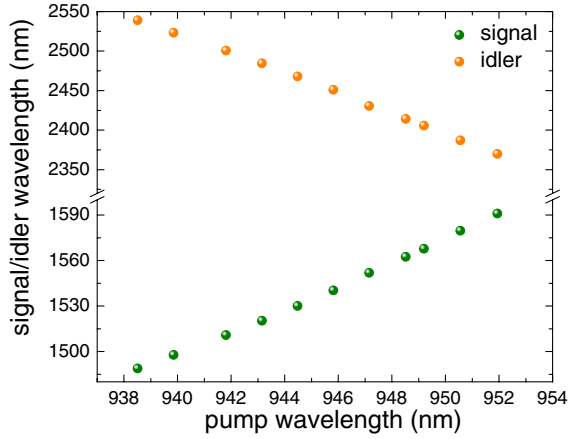

Fig. 4. Tuning of signal and idler wavelengths as functions of the pump wavelength. The idler wavelength is obtained using the conservation of energy $1/\lambda_i = 1/\lambda_p - 1/\lambda_s$ from the pump and signal wavelengths.

170 nm for the idler was achieved. The internal normalized efficiency of the device was estimated to be 0.29% $W^{-1}\,cm^{-2}$. The reported device is attractive for applications where a large wavelength tunability of an IR source between 2 and 3 μm wavelength is desired on a chip form factor.

References

1. HITRAN web site, http://cfa-www.harvard.edu/hitran/.
2. A. Farooq, J. B. Jeffries, and R. K. Hanson, Meas. Sci. Technol. **19**, 075604 (2008).
3. M. G. Allen, Meas. Sci. Technol. **9**, 545 (1998).
4. A. Joullié and P. Christol, C. R. Phys. **4**, 621 (2003).
5. M. Razeghi, IEEE J. Sel. Top. Quantum Electron. **15**, 941 (2009).
6. R. F. Curl, F. Capasso, C. Gmachl, A. A. Kosterev, B. McManus, R. Lewicki, M. Pusharsky, G. Wysocki, and F. K. Tittel, Chem. Phys. Lett. **487**, 1 (2010).
7. A. Vizbaras, M. Anders, C. Grasse, S. Katz, G. Boehm, R. Meyer, M. A. Belkin, and M.-C. Amann, Phys. Status Solidi C **9**, 298 (2012).
8. S. D. Jackson, Nat. Photonics **6**, 423 (2012).
9. R. L. Byer, J. Nonlinear Opt. Phys. Mater. **6**, 549 (1997).
10. P. Bravetti, A. Fiore, V. Berger, E. Rosencher, J. Nagle, and O. Gauthier-Lafaye, Opt. Lett. **23**, 331 (1998).
11. R. Haidar, A. Mustelier, P. Kupecek, E. Rosencher, R. Triboulet, P. Lemasson, and G. Mennerat, J. Appl. Phys. **91**, 2550 (2002).
12. P. Abolghasem, J.-B. Han, D. Kang, B. J. Bijlani, and A. S. Helmy, IEEE J. Sel. Top. Quantum Electron. **18**, 812 (2012).
13. J. B. Han, P. Abolghasem, D. Kang, B. J. Bijlani, and A. S. Helmy, Opt. Lett. **35**, 2334 (2010).
14. P. Abolghasem and A. S. Helmy, J. Opt. Soc. Am. B **29**, 1367 (2012).
15. P. Abolghasem, J. Han, B. J. Bijlani, and A. S. Helmy, Opt. Express **18**, 12681 (2010).
16. A. Fiore, V. Berger, E. Rosencher, P. Bravetti, N. Laurent, and J. Nagle, Appl. Phys. Lett. **71**, 3622 (1997).
17. O. Levi, T. J. Pinguet, T. Skauli, L. A. Eyres, K. R. Parameswaran, Jr., J. S. Harris, and M. M. Fejer, Opt. Lett. **27**, 2091 (2002).
18. T. H. Stievater, R. Mahon, D. Park, W. S. Rabinovich, M. W. Pruessner, J. B. Khurgin, and C. J. K. Richardson, Opt. Lett. **39**, 945 (2014).